International Research Journal of Advanced Engineering and Science
ISSN (Online): 2455-9024

Investigation on Flow Characteristics of Backward-facing Step Flow in a Rectangular Duct using Stereo PIV

Shuai Zou, Shogo Motoda, Kyoji Inaoka
Department of Mechanical Engineering, Doshisha University, Kyotanabe 610-0321, Japan

Abstract— *The spatial distribution of the velocity component and local heat transfer coefficient on the bottom wall downstream of the backward-facing step in a duct flow was measured using the stereo particle image velocimetry (PIV) method and a thermo-sensitive liquid crystal sheet, respectively. A heat transfer experiment and three components of the time-averaged velocity measurement by stereo PIV were performed for a Reynolds number of 900 for the stepped duct with an aspect ratio of 16 and expansion ratio of 2. The local Nusselt number varies in the flow and spanwise directions; that is, the maximum Nusselt number always appears near the sidewall region. The heat transfer coefficient downstream of the reattached region is slightly high. Areas with large fluctuations conform well with the suitable heat transfer areas. The maximum heat transfer area is on the side wall owing to the strong flow fluctuations. The velocity fluctuation intensity increases downstream, and the flow fluctuates greatly with increase in time.*

Keywords— *Backward-Facing Step; Flow Reattachment; Stereo PIV; Three-Dimensional Flow.*

I. INTRODUCTION

Separation and reattachment flow phenomena can be observed in various thermo-fluid devices. In addition, because a high heat transfer coefficient can be obtained at the reattachment position, it is important to understand this phenomenon in the field of engineering. Backward-facing step (BFS) flow is one of the simplest flow systems that can achieve separation and reattachment. Currently, basic studies on the flow and heat transfer characteristics of the BFS flow have been conducted [1]. However, most of these conventional studies have been conducted with a high aspect ratio by setting a sufficient length of the flow path in the spanwise direction. Simply, it is considered that the two-dimensionality of the flow field behind the step is maintained when the width of the flow path is widened, and research on the reattachment position and heat transfer characteristics is conducted focusing only on the center of the flow path. (Eaton et al., 1981) [2]. However, several steps used in actual thermo-fluid equipment are internal flows with side walls, the influence of which cannot be neglected. Therefore, research on the effect of the side wall on the flow field has been actively conducted, but the flow structure of the step flow in the internal flow represented by the rectangular duct is complicated, unlike the step flow, which assumes two-dimensionality. Suyama et al. [3] experimentally investigated the fluctuation of velocity field and reattachment position near the bottom wall downstream of the step in the Reynolds number (*Re)* region, from the laminar to the transition flow region, using a duct with an aspect ratio of 16 [3]. Consequently, the reattachment position in the center of the flow path on the bottom wall surface diverges from the step as the *Re* increases and approaches the step after the *Re* is 400. Furthermore, the phenomenon in which the flow becomes unsteady after *Re* 400 is clarified. However, it was not possible to obtain details of the relationship between flow and heat transfer in the relatively low *Re* region. Inaoka et al. [4] conducted heat transfer experiments in a wide *Re* region, from laminar flow to turbulent flow, and measured the local heat transfer coefficient of the bottom wall surface behind the step [4]. They reported that the value of the heat transfer coefficient downstream of the step in the duct changed significantly in the spanwise direction and the maximum heat transfer coefficient appeared near the side wall, which was caused primarily by the flow down washing from the side wall. In addition, our group conducted an experiment at *Re* of 400, where unsteady flow is evident, and obtained the result of the movement of the instantaneous reattachment position and the movement of the lateral vortex generated in the circulation region. In addition, the velocity by particle image velocimetry (PIV) was measured in the low-*Re* region (400 to 900), and the complexity of the flow in the spanwise direction increased as the *Re* increased with the local heat transfer coefficient on the bottom wall surface. It was clarified that both the flow and heat transfer regions with high variability have a similar relationship. However, there have been few reports on the complexity of the flow in the spanwise direction, the relationship between the secondary flow and heat transfer appearing near the bottom wall, and the three-dimensional flow structure of the secondary flow. Therefore, in this study, to consider the three-dimensional flow at a low *Re* (900), the stereo PIV method that measures the three velocity components, including the velocity in the depth direction in the two-dimensional plane, was adopted. Thereafter, the flow velocity is measured behind the step and near the side wall, before and after the reattachment position, to obtain a flow structure in the flow, spanwise, and height directions. The characteristics of this flow were investigated. In addition, the fluctuation intensity was calculated for the velocities of flow, height, and spanwise directions from the time series data of the velocity. The relationship between the flow structure and heat transfer was considered with the results of heat transfer experiments using a thermo-sensitive liquid crystal method, which exhibits coloration depending on temperature.

Shuai Zou, Shogo Motoda, and Kyoji Inaoka, "Investigation on Flow Characteristics of Backward-facing Step Flow in a Rectangular Duct using Stereo PIV," *International Research Journal of Advanced Engineering and Science*, Volume 5, Issue 4, pp. 86-94, 2020.

International Research Journal of Advanced Engineering and Science
ISSN (Online): 2455-9024

II. Experimental Apparatus and Procedures

A. Experimental Flow Path

Fig. 1 demonstrates a schematic diagram of the experimental equipment. In this study, the working fluid is water, which is stored in the downstream tank ①, and then is pumped up to the upstream tank ③ using a circulation pump ②. In the upper tank, when the working fluid exceeds a certain amount, it is returned to the downstream tank. Thereafter, the working fluid flows into the rectifying section ⑥ through the straw pipes, crosses this section, and enters the developing section ⑧ after the cross section is reduced to 1/12 by contraction section ⑦. The length of the developing section was 1500 mm. In the developing section, the working fluid becomes a fully-developed flow and flows into the test section ⑨. After traversing the test section, the working fluid flows into the downstream tank again. The flow rate is measured using a flow meter ⑪ (manufactured by Nippon Flowcell Co., Ltd., SAG-1 type) installed behind the test section.

B. Test Section

Fig. 2 depicts a schematic diagram of the test section, which is a rectangular duct with a spanwise direction length of W_D = 240 mm and a flow path height of H = 30 mm, and the internal step height is S = 15 mm. The aspect ratio is 16, and the expansion ratio is 2. The origin of the coordinate axes is the center position in the spanwise direction at the bottom of the step; the *x*-axis, *y*-axis, and *z*-axis are in the flow, height, and spanwise directions. In the following description, for the *x*-axis and *y*-axis values, *x/S* and *y/S* are dimensionless with the step height *S*. For the *z-axis* value, z/W_D is dimensionless with the duct width W_D.

C. Visualization Experiment Method Using Stereo PIV

Fig. 3 illustrates a schematic diagram of the camera layout used in the stereo PIV method. In the visualization experiment, a green laser (LASER QUANTUM, opus, output 1.0 W) was developed into a sheet with a thickness of 0.7 to 0.9 mm by mixing nylon particles (particle diameter 48 to 52 μm) in the working fluid, and then tested. The section was illuminated and photographed using two high-speed cameras (KANOMAX, FASTCAM Mini AX). The laser irradiation cross-section was the *y-z* cross-section. Therefore, the velocity component u in the mainstream direction is measured as the third component perpendicular to the cross-section. The angle between the two cameras was set to 60°, and the cameras were arranged to satisfy the shining condition, where the sheet light, lens main plane, and extension line of the imaging surface intersection. In addition, to cancel the effect of refraction on the side wall of the flow path, a triangular water tank filled with water was attached to the side wall, through which the images were captured.

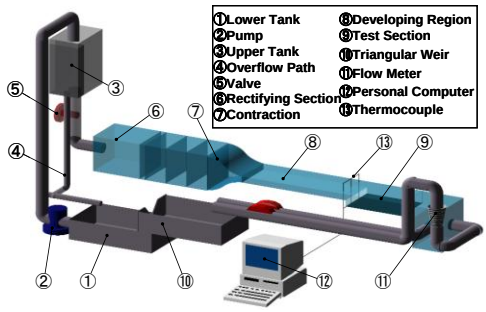

Fig. 1. Closed water channel used in the present study.

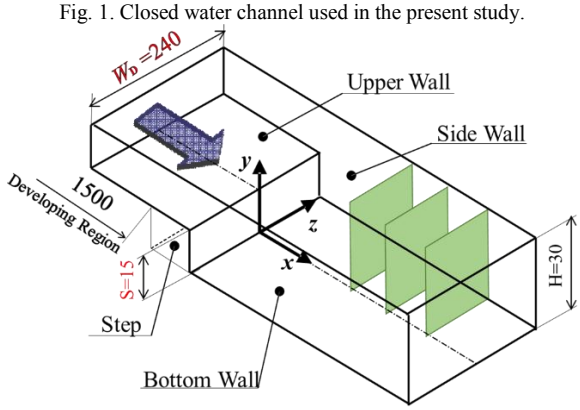

Fig. 2. Test section of a backward-facing step flow in a duct.

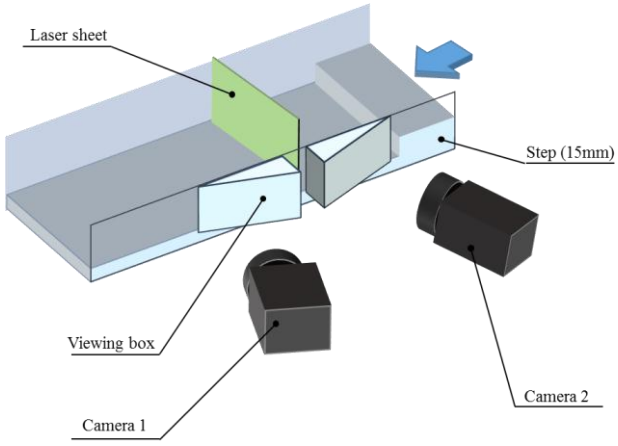

Fig. 3. Illustration of the stereo PIV experiment.

D. Definition of Dimensionless Number

In this study, the *Re* was defined using the cross-sectional average velocity U_{m0} and step height *S* as the representative velocity and representative length, respectively, as shown in (1), and the experiment was conducted under the condition that *Re* = 900.

$$Re = \frac{U_{m0} \cdot S}{\nu} \quad (1)$$

Here, ν represents the kinematic viscosity of water, m^2/S.

E. Speed Measurement

The velocity distribution was measured as follows: Nylon particles were mixed in the working fluid, and a sheet-shaped high-intensity green laser was irradiated on the *y-z* cross section, as shown in Figs. 2 and 3 to visualize it; the scattered light of the particles was photographed using a high-speed camera. The velocity distribution was obtained from the

Shuai Zou, Shogo Motoda, and Kyoji Inaoka, "Investigation on Flow Characteristics of Backward-facing Step Flow in a Rectangular Duct using Stereo PIV," *International Research Journal of Advanced Engineering and Science*, Volume 5, Issue 4, pp. 86-94, 2020.

International Research Journal of Advanced Engineering and Science
ISSN (Online): 2455-9024

captured images using the cross-correlation PIV method (LaVision, Davis 10.0.4). The imaging area in the y and z directions was 1024 pixels for each direction, and 1 pixel represents 0.05 mm. In general, it is preferable for the particle image size to be 2 to several pixels, the number of particles in the inspection area to be approximately 5, and the moving distance of the particles to be within 5 pixels [5-8]. Accordingly, the experiment was conducted by setting the frame rate of the high-speed camera as 130 fps and the number of shots as 1000. In this study, the inspection area was 16 × 16 pixels, and the exploration area was 32 × 32 pixels.

F. Measurement Accuracy of Speed Experiment

The validity of the velocity experiment in the stereo PIV method is examined in this section. Fig. 4 presents the velocity distribution map of the center of the flow path in the rectangular flow path area on the upstream side of the step position. The laser sheet irradiates the y-z cross section and compares the time average value of the mainstream velocity component u obtained as the velocity component perpendicular to the cross section with the velocity distribution equation [9] in the rectangular flow path. As for the coordinate axis, the vertical axis represents the velocity component u in the flow direction divided by the cross-sectional average flow velocity U_{m0} at the inlet, and the horizontal axis represents the flow height direction y/S. The average relative error from the theoretical formula was approximately 4% for x/S = 0.0 and x/S= –0.1. Next, Fig. 5 (a) and (b) demonstrate the velocity distribution map at z/W_D= 0.3 with a Re of 900 at the positions x/S = 10.0 and x/S = 12.0. The results of irradiating the x-y cross section and y-z cross section with a laser sheet and photographing by the stereo PIV method are compared with the results of 2D-PIV reported by Shuai Zou et al. [10]. For the coordinate axes, the vertical axis represents the velocity component u in the flow direction divided by the cross-sectional average flow velocity U_{m0} at the inlet, and the horizontal axis represents the flow path height direction y/S. The average relative error value is approximately 5% and 6% at positions x/S = 10.0 and x/S = 12.0, respectively, because of experimental errors, such as flow rate adjustment and difference in average time.

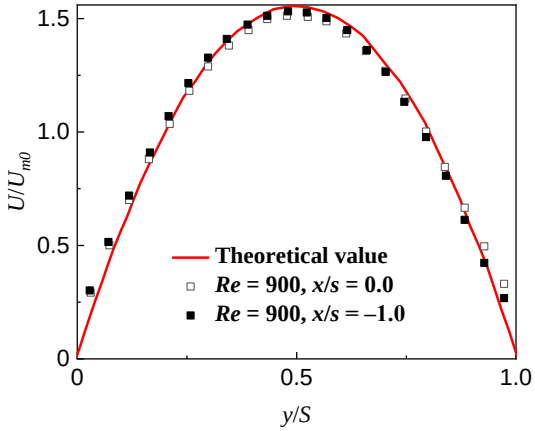

Fig. 4. Velocity distribution of x/S = 0.0 and −0.1, z/W_D= 0.0 for Re = 900.

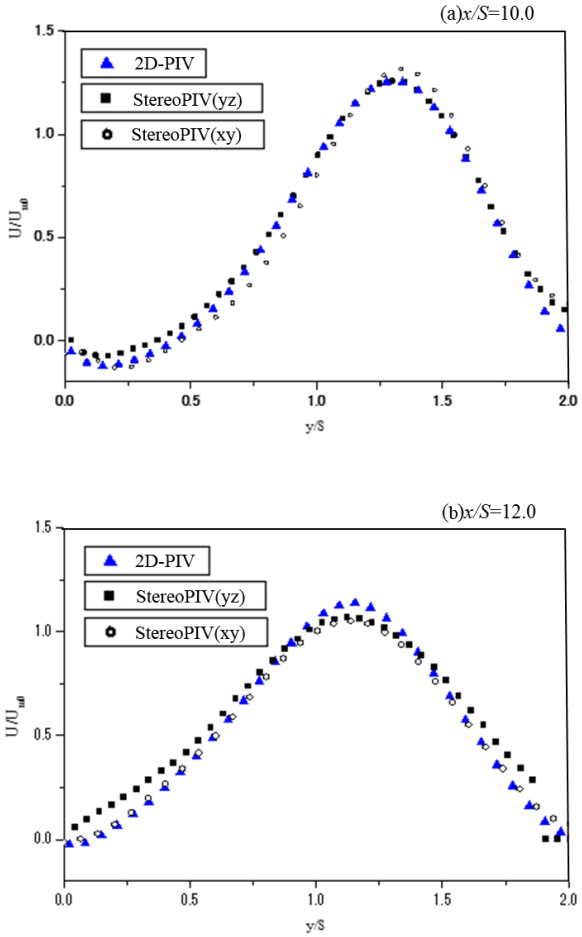

Fig. 5. Velocity distribution of mainstream direction at x/S = (a) 10.0 and (b) 12.0 for Re = 900.

III. Results and Considerations

A. Local Nusselt Number Distribution

Fig. 6 illustrates the contour distribution map of the local Nusselt number on the bottom wall surface at a Re of 900 as reported by Shuai Zou et al. [10]. For the coordinate axes, the horizontal and vertical axes indicate the flow (x-axis direction) and spanwise directions (z-axis direction), respectively. In the color contour, red and blue indicate the regions where the Nusselt number values are high and low, respectively. In addition, the distribution of the time-averaged reattachment position in the z direction obtained from the time-averaged velocity at the position y = 0.05 near the bottom wall surface is indicated by a small circle. Moreover, Fig. 7 presents the distribution map of the local Nusselt number for each x/S at an Re of 900 reported by Zou et al.[10]. The horizontal and vertical axes represent the spanwise direction and the local Nusselt number, respectively. Furthermore, Figs. 6 and 7 show the region from z/W_D = 0.17 near the center of the flow path to z/W_D = 0.5 on the side wall. As shown in Fig. 6, the value of the local Nusselt number is low in the circulation region upstream of the reattachment position, and then gradually increases and reaches its peak after the reattachment point. It

Shuai Zou, Shogo Motoda, and Kyoji Inaoka, "Investigation on Flow Characteristics of Backward-facing Step Flow in a Rectangular Duct using Stereo PIV," *International Research Journal of Advanced Engineering and Science*, Volume 5, Issue 4, pp. 86-94, 2020.

International Research Journal of Advanced Engineering and Science
ISSN (Online): 2455-9024

can also be observed that the distribution of local Nusselt numbers changes in the spanwise direction and exhibits a high value near the side wall. In Fig. 7, the highest local Nusselt number is z/W_D = 0.2 to 0.3 at x/S = 11.00; at z/W_D = 0.4, it enters the heat transfer deterioration region, and at approximately z/W_D = 0.45, it shows the maximum value around. In the region of x/S = 12.00 to 12.75, low values are shown at approximately z/W_D = 0.4 to 0.45, and high values of local Nusselt numbers are shown between z/W_D = 0.3 and 0.45 to 0.5. Furthermore, the value of the local Nusselt number in the entire spanwise direction increases toward the downstream. After x/S = 13.50, the poor heat transfer region of z/W_D = 0.4 to 0.45 disappears, showing a higher value of the local Nusselt number near the side wall than the center. The flow structure near the side wall is considered to change on the upstream and downstream sides of x/S = 13.50, and thus, it is necessary to examine the characteristics of the flow in detail.

B. *Average Velocity Distribution of Each Cross Section*

The flow field was measured using the stereo PIV method at a *Re* of 900. Figs. 8 (a) to (h) demonstrate the mean velocity distribution obtained by dividing the velocity component u in the x direction of the y-z cross section by the cross-sectional average flow velocity U_{m0} at the inlet. The color contour shows high values for red and low values for blue, as well as the value of u/U_{m0} = 0.0. Therefore, the region where the flow velocity is negative outside the contour line is the circulation region before reattachment. As the cross section moves toward the wake side, the circulation area near the bottom wall decreases and eventually disappears. Because the circulation region has almost disappeared between x/S = 11.50 and 12.00, a time-averaged reattachment position exists in this region, which is considered valid when compared with that in the *Re* of 900. In addition, the disappearance of the circulation region at approximately z/W_D = 0.45 from x/S = 11.50 to 12.00 is consistent with the phenomenon that the time-averaged reattachment position projects upstream near the side wall.

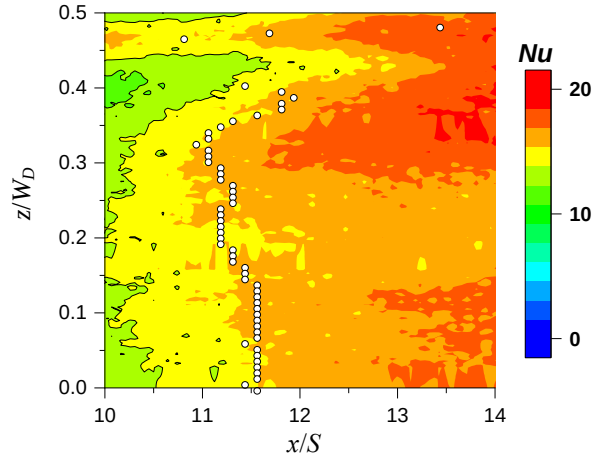

Fig. 6. Distribution of the local Nusselt number on the bottom wall for *Re* = 900.

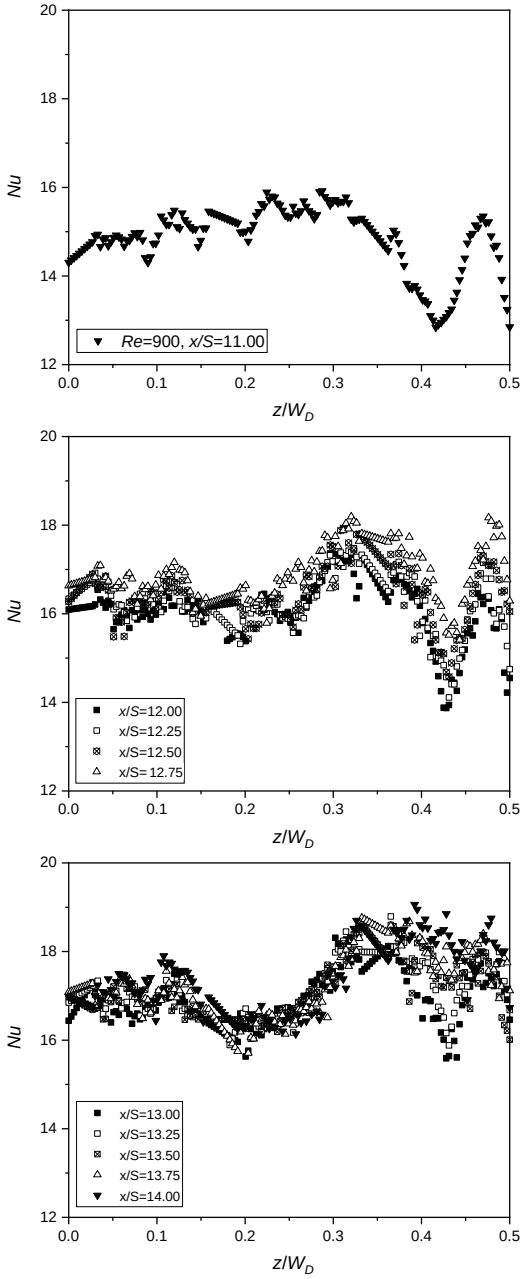

Fig. 7. Distribution of the local Nusselt number on the bottom wall for x/S = 11,12,13,14.

C. *Time-averaged Velocity Vector Diagram in Each Cross Section*

Figs. 9 and 10 superimposed the distribution of the flow direction component u/U_{m0} with the average velocity vector $\bar{V} - \bar{W}$ of the y-z section from x/S = 12.00 to 14.00 with *Re* = 900. First, observing the flow near the side wall in Fig. 9 (a) to (c), the flow from the center of the flow path bounced off the side wall collide and are strong toward the bottom wall at approximately z/W_D = 0.45. In the heat transfer experiment conducted by Inaoka et al. [11], it has been reported that there is a strong flow toward the bottom wall near the side wall called a downwash flow, which has a significant influence on heat transfer (Inaoka et al., 2013).

Shuai Zou, Shogo Motoda, and Kyoji Inaoka, "Investigation on Flow Characteristics of Backward-facing Step Flow in a Rectangular Duct using Stereo PIV," *International Research Journal of Advanced Engineering and Science*, Volume 5, Issue 4, pp. 86-94, 2020.

International Research Journal of Advanced Engineering and Science
ISSN (Online): 2455-9024

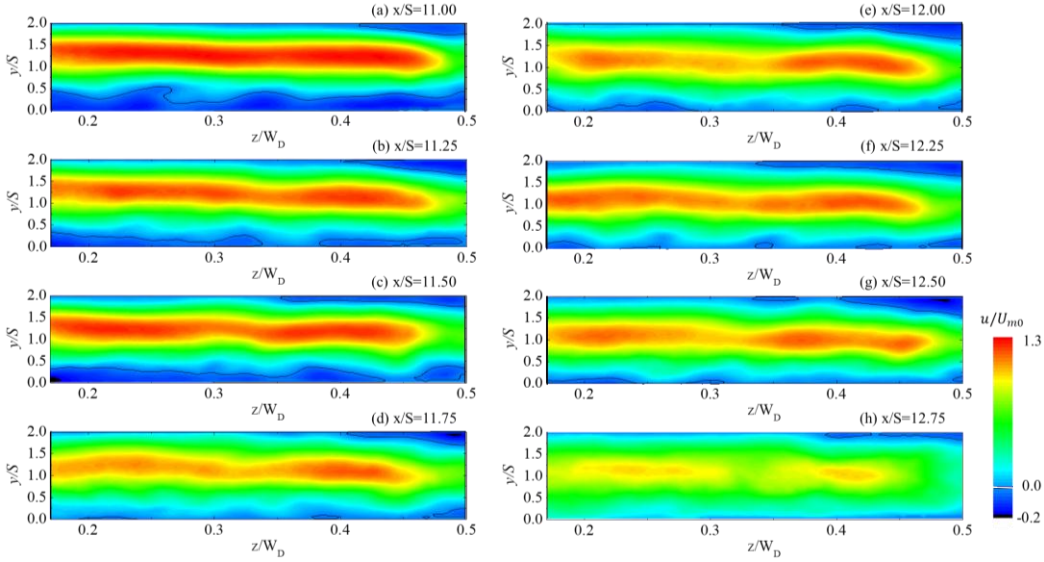

Fig. 8. Mean velocity distribution in the main flow direction of *Re* = 900 for each *y*-*z* plane.

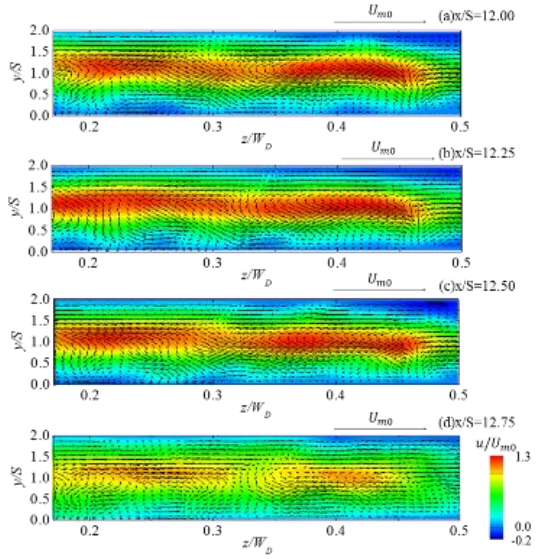

Fig. 9. Cross-sectional distribution of the time-averaged velocity vectors for each *y*-*z* plane and mean velocity distribution in the main flow direction for *Re* = 900.

The strong flow to the bottom wall generated by the collision of the flow from the center of the flow path and the flow from the side wall is considered to be the flow equivalent to the downwashflow. It can also be observed that the flow in the mainstream direction is strong in the region where this collision flow occurs. Therefore, in the region x/S = 12.00 to 12.50, we can infer that the collision of the flow from the center of the flow path and the flow from the side wall strengthens the flow toward the bottom wall and that in the mainstream direction. Focusing on the flow near z/W_D = 0.42, which exhibited a low local Nusselt number, as described in subsection A of this section. There exists a region where the flow velocity in the mainstream direction is small and there is no strong flow in the spanwise or height directions. It is believed that this slow flow field hinders the promotion of heat transfer. Furthermore, examining the flow near z/W_D = 0.3, the flow from the center of the flow path and the flow from the side wall collide with each other near the upper wall, and a strong flow toward the bottom wall is generated. It is considered that this collision strengthens the flow in the spanwise direction near the bottom wall and promotes heat transfer from z/W_D = 0.3 to 0.4.

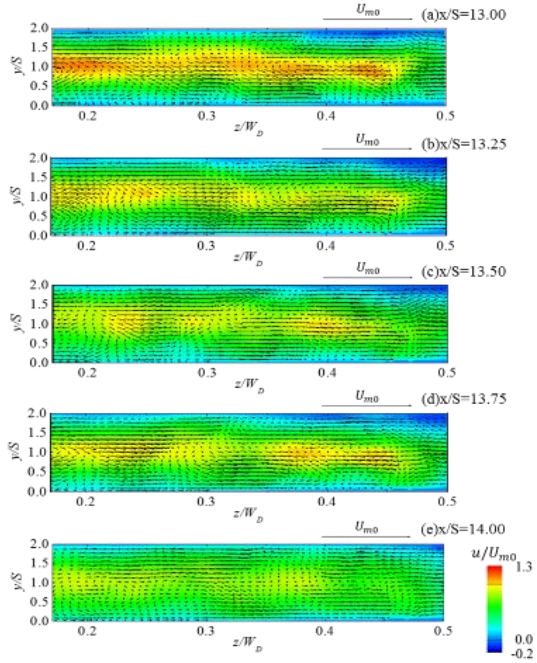

Fig. 10. Cross-sectional distribution of the time-averaged velocity vectors for each *y*-*z* plane and mean velocity distribution in the main flow direction for *Re* = 900.

In Fig. 10 (a) to (e), the phenomenon that the flow from the side wall and the flow from the center of the flow path collide can be confirmed, but it is lower than the upstream x/S = 12.00 to 12.75. The flow toward the wall is observed to be weakened. Moreover, it can be confirmed that for the flow in the mainstream direction, the flow velocity near the bottom

Shuai Zou, Shogo Motoda, and Kyoji Inaoka, "Investigation on Flow Characteristics of Backward-facing Step Flow in a Rectangular Duct using Stereo PIV," *International Research Journal of Advanced Engineering and Science*, Volume 5, Issue 4, pp. 86-94, 2020.

International Research Journal of Advanced Engineering and Science
ISSN (Online): 2455-9024

wall increases toward the downstream, and the difference between the fast and slow flow regions becomes small. The reason why the poor heat transfer region of z/W_D = 0.4 to 0.45 disappears is because there is no region with a small flow velocity in the mainstream direction. Because the flow that blows down to the bottom wall exists in the entire region of x/S = 12 to 14, the region of z/W_D = 0.3 to 0.5 is larger than the region of z/W_D = 0.2 to 0.3, near the center of the flow path; the value of the heat transfer coefficient is considered larger in that case.

C. *Velocity Fluctuation Intensity in Each Cross Section*

Fig. 11 presents a diagram in which the fluctuation intensity of each flow direction component is divided by the cross-sectional average flow velocity at the inlet. First, we focus on the fluctuation intensity in the mainstream direction. The region where the fluctuation intensity value is large increases toward the downstream, and the fluctuation intensity increases significantly at the boundary of x/S = 13.00 in the region near the side wall of z/W_D = 0.4 to 0.5. The average velocity distribution in the mainstream direction stabilizes and approaches the shape of the developed flow from the reattachment position toward the downstream, but the fluctuation intensity increases.

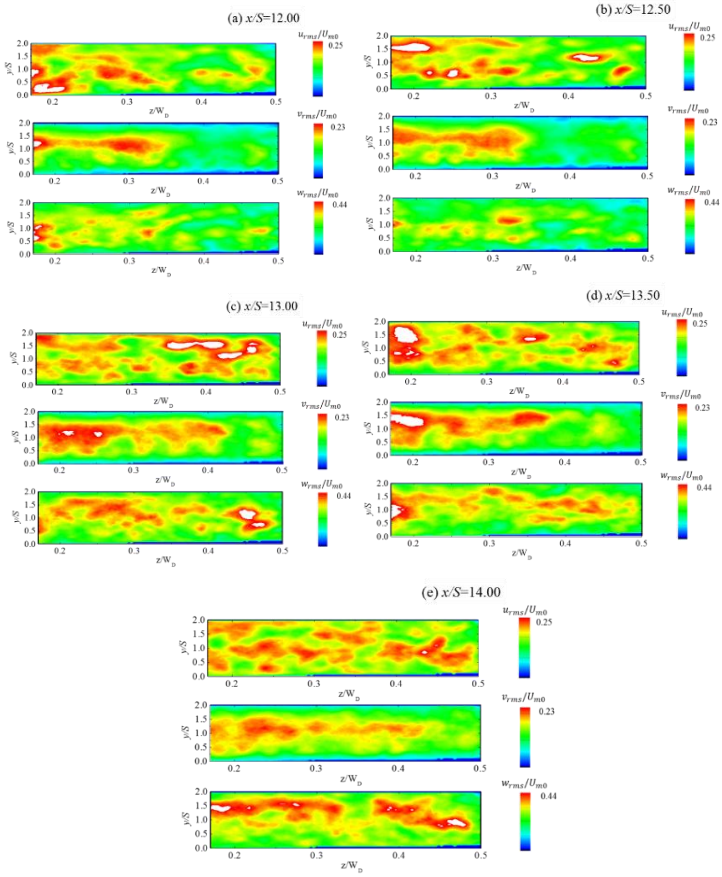

Fig. 11. Velocity fluctuation intensity distribution of the time averaged for each *y*-*z* plane.

Thus, it can be inferred that this increase in fluctuation intensity contributes to the increase in the heat transfer coefficient in the mainstream direction. For the fluctuation intensity in the height direction, we can observe a region with a large fluctuation intensity centered on z/W_D = 0.3 and y/S = 1.0. This is almost similar to the region where the strong flow toward the bottom wall generated by the collision flow exists, and it is expected that this flow fluctuates with time in the height direction. In addition, there is a strong flow that blows down to the bottom wall even in the region where the fluctuation intensity of z/W_D = 0.4 to 0.5 is low, which indicates that the strong flow is constant without significant time fluctuation. In the region of z/W_D = 0.4 to 0.5, there is no significant increase in fluctuation intensity toward the downstream. Focusing on the fluctuation intensity in the spanwise direction, it can be confirmed that the turbulent intensity increases significantly at the boundary of x/S = 13.00. From the time-averaged velocity vector diagram, it seems that the flow velocity in the spanwise direction decreases toward the downstream, but because the fluctuation intensity increases, a time-varying flow exists over the entire spanwise direction.

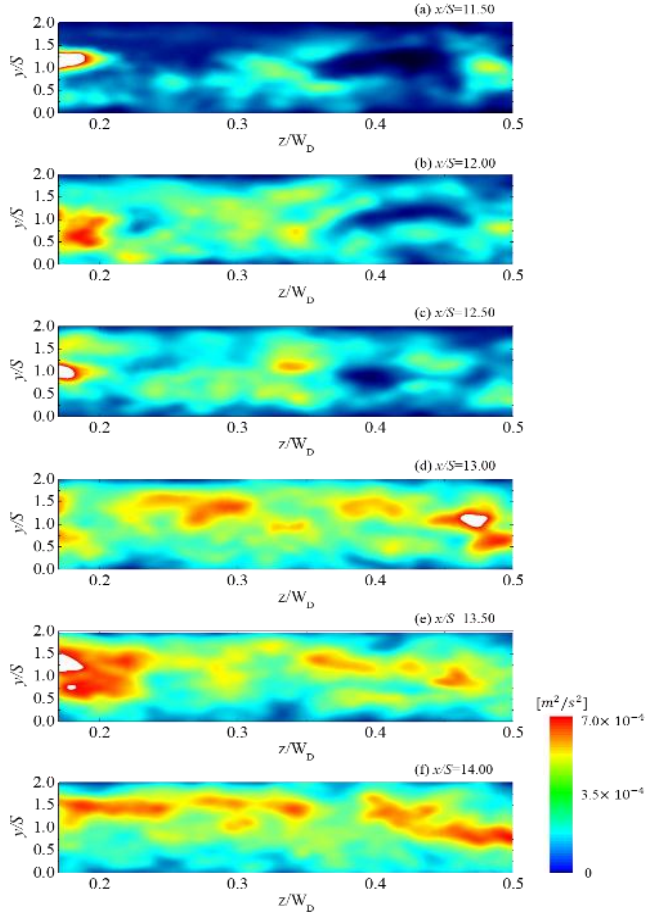

Fig. 12. Turbulent kinetic energy distribution for each *y*-*z* plane.

D. *Turbulent Kinetic Energy in Each Cross Section*

Fig. 12 illustrates the magnitude of the turbulent energy in the cross section of each *y*-*z* plane from x/S = 11.50 to 14.00. It can be confirmed that the turbulent energy of the entire cross section increases toward the downstream, and the value increases particularly in the region near the side wall of z/W_D = 0.4 to 0.5. Accordingly, it is considered that the turbulence

Shuai Zou, Shogo Motoda, and Kyoji Inaoka, "Investigation on Flow Characteristics of Backward-facing Step Flow in a Rectangular Duct using Stereo PIV," *International Research Journal of Advanced Engineering and Science*, Volume 5, Issue 4, pp. 86-94, 2020.

International Research Journal of Advanced Engineering and Science
ISSN (Online): 2455-9024

of the flow increases after passing the reattachment position, and the downwash flow that appears near the side wall changes to a flow that fluctuates with time at approximately x/S = 13.00. Furthermore, despite focusing on the vicinity of the bottom wall, the turbulent energy for each cross section increases toward the downstream, and the ratio of heat transport is observed to increase owing to the turbulence of the flow.

E. Momentum Transport to the Bottom Wall Surface in Each Cross Section

Fig. 13 presents the distribution map of the Reynolds stress $-\overline{uv}$ in each y-z cross section, where v represents the wall normal velocity. Here, positive and negative values indicate the magnitude of momentum transport toward the bottom wall and the upper wall, respectively. From this distribution, there are regions with large momentum transport to the bottom wall and the upper wall surfaces, with similar sizes on the bottom wall and upper wall sides of the flow path. However, it can be observed that the size of this region and the tendency of the values do not change significantly between the upstream and downstream sides. Therefore, it can be inferred that the momentum transport to the bottom wall surface by the flow in the mainstream direction does not significantly affect the increase in the heat transfer coefficient of the bottom wall surface from x/S = 12.00 to 14.00.

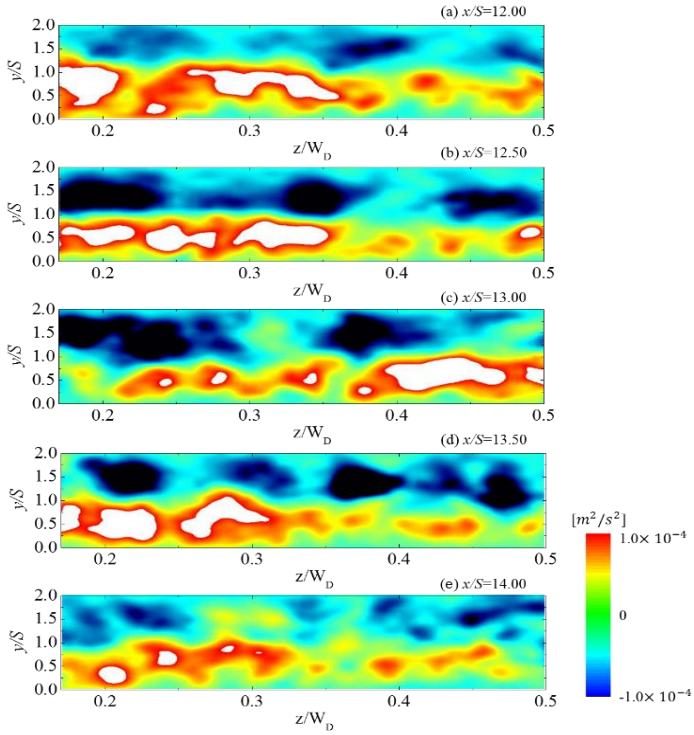

Fig. 13. Reynolds stress distribution for each y-z plane.

F. Instantaneous Diagram of Velocity Vector and Vorticity Due to Fluctuation Components

Fig. 14 illustrates the time-averaged velocity distribution in the height direction at x/S =13.75 and 14.00. It can be observed that the velocity gradient is large in the region around z/W_D = 0.25 to 0.35 in both cross-sections near the bottom wall surface. Because it is believed that vortices are likely to occur at positions where this velocity gradient is large, we focus on the vortex structure that occurs in the region near z/W_D = 0.3 in the instantaneous velocity vector diagram. Fig. 15 and 17 present the instantaneous velocity vector diagram when the vortex structure was observed at x/S = 13.75 and 14.00 and the superposition diagram of the vorticity distribution calculated by the velocity fluctuation component.

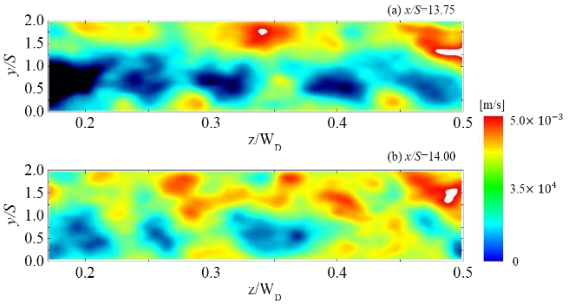

Fig. 14. Velocity distribution for each y-z plane.

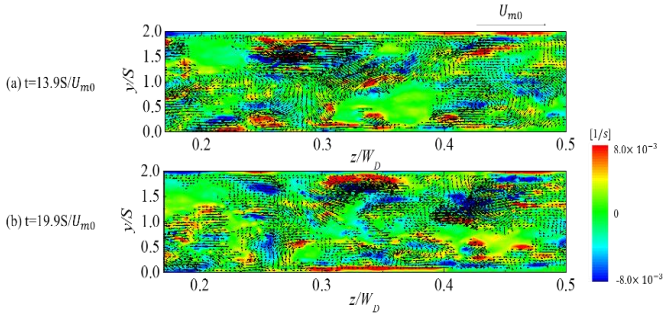

Fig. 15. Instantaneous velocity vectors and instantaneous vorticity in y-z plane at x/S = 13.75.

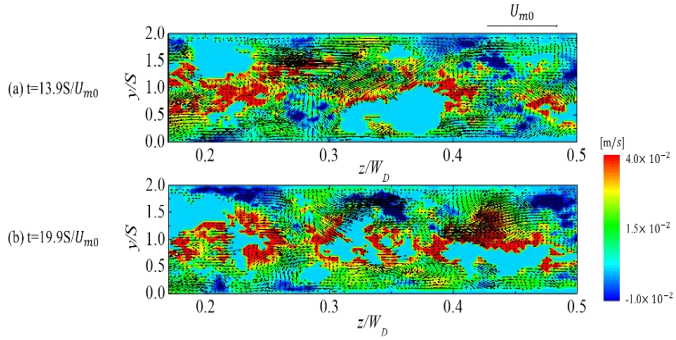

Fig. 16. Instantaneous velocity vectors and instantaneous velocity component in y-z plane at x/S = 13.75.

Fig. 16 to 18 demonstrate a superposition of the instantaneous velocity vector diagram and instantaneous vorticity distribution of the mainstream direction components simultaneously. From these figures, the vortex structure appearing in the region of z/W_D = 0.25 to 0.3 is primarily counterclockwise when viewed from the downstream direction and clockwise in the region of z/W_D = 0.3 to 0.35. It can also be confirmed that the counterclockwise and clockwise vortex structures have negative and positive velocity components, respectively, with respect to the mainstream direction. Focusing on the flow near the upper wall, it can be observed that the flow from the center of the flow path and the flow

Shuai Zou, Shogo Motoda, and Kyoji Inaoka, "Investigation on Flow Characteristics of Backward-facing Step Flow in a Rectangular Duct using Stereo PIV," *International Research Journal of Advanced Engineering and Science*, Volume 5, Issue 4, pp. 86-94, 2020.

from the side wall direction collided with each other to generate a strong flow toward the bottom wall. The position where this flow collides appears at approximately z/W_D = 0.3 and 0.4. In addition, it is considered that this collision and the flow toward the bottom wall generate a vortex structure.

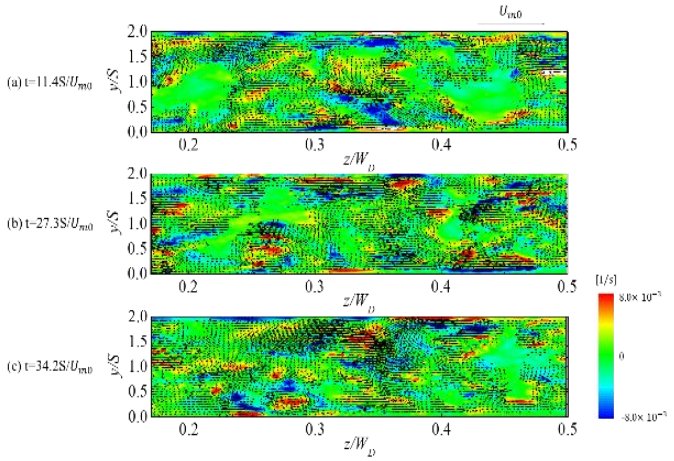

Fig. 17. Instantaneous velocity vectors and instantaneous vorticity in *x-y* plane at x/S = 14.00.

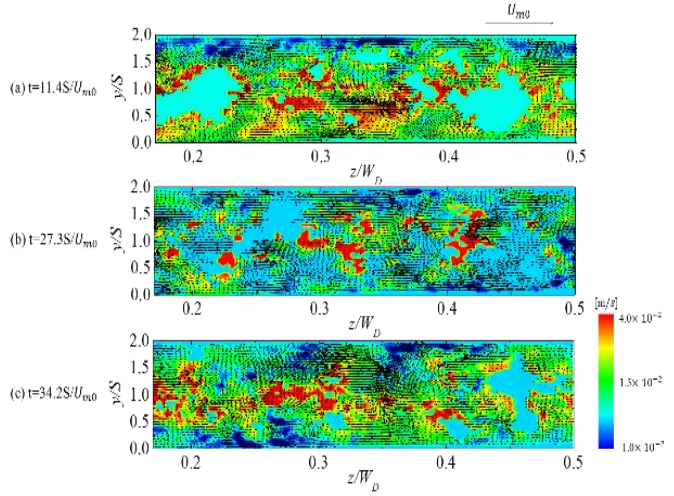

Fig. 18. Instantaneous velocity vectors and instantaneous velocity component in *x-y* plane at x/S = 14.00.

IV. Conclusion

In this study, the spatial distribution of the velocity component downstream of the backward-facing step in a duct flow was measured using the stereo PIV method. The spatial distribution of the local heat transfer coefficient on the bottom wall downstream of a backward-facing step in a duct flow was measured by a thermo-sensitive liquid crystal sheet. A heat transfer experiment and three components of the time-averaged velocity measurement by stereo PIV were performed for *Re* of 900 for the stepped duct with aspect and expansion ratios of 16 and 2, respectively. The primary results obtained from this study are summarized as follows:

(1) The value of the heat transfer coefficient gradually increases downstream of the reattached region, changes in the spanwise direction, and increases from the center of the channel to the side wall. In the upstream at x/S = 13.75, a poor heat transfer area exists around z/W_D = 0.45.

(2) In the region where the heat transfer coefficient is high near the side wall, there is a strong flow that blows down to the bottom wall, caused by the collision between the flow from the center of the flow channel and the flow that rebounds and hits the side wall. In the region where the heat transfer coefficient is low, the flow is slow in the main flow, height, and spanwise directions for certain areas.

(3) The turbulence kinetic energy in the section increases as the flow goes downstream. The fluctuation near the side wall increases after x/S=13.0, and the downwash flow fluctuates at time. In addition, the fluctuation of the particularly mainstream direction and spanwise direction affects it. As the strength of these changes increases, the value of the heat transfer coefficient increases.

(4) In the domain where the speed gradient of the height direction is large at x/S = 13.75 and 14.00, vorticity repeats outbreak and extinction. The whirlpool structure appears at z/W_D = 0.25 to 0.3, which has a regular velocity component in the mainstream direction, and the vorticity appears in z/W_D = 0.3 to 0.35, which has a negative velocity component in the mainstream direction. This vorticity occurs by the strong flow to the bottom wall, which is the flow from the center of the duct and the flow from the side wall near the upper wall.

Acknowledgment

The first author Shuai Zou gratefully acknowledges the financial support from China Scholarship Council (CSC) (No.201808320398), which has sponsored his Ph.D. study at the Doshisha University in Japan.

References

[1] E. W. Adams and J. K. Eaton, "An LDA Study of the Backward-Facing Step Flow, Including the Effects of Velocity Bias," *Journal of Fluids Engineering,* vol. 110, no. 3, pp. 275–282, 1988, doi: 10.1115/1.3243545.

[2] B. F. Armaly, F. Durst, J. Pereira, and B. Schönung, "Experimental and theoretical investigation of backward-facing step flow," *Journal of fluid Mechanics,* vol. 127, pp. 473–496, 1983.

[3] N. Suyama, K. Inaoka, and M. Senda, "Flow Characteristics Over a Backward-Facing Step in a Duct in Low Reynolds Number Range," in *ASME/JSME 2011 8th Thermal Engineering Joint Conference*, Honolulu, HI, 2011. Available: https://doi.org/10.1115/AJTEC2011-44246

[4] K. Inaoka and M. Senda, "Heat Transfer and Fluid Flow Characteristics of a Backward-Facing Step Flow in a Duct," *Transactions of the Japan Society of Mechanical Engineers Series B,* vol. 79, no. 804, pp. 1651–1663, 2013, doi: 10.1299/kikaib.79.1651.

[5] K. Shinohara, Y. Sugii, A. Aota, A. Hibara, M. Tokeshi, T. Kitamori, and K. Okamoto, "High-speed micro-PIV measurements of transient flow in microfluidic devices," *Measurement science and Technology,* vol. 15, no. 10, p. 1965, 2004.

[6] D. J. White, W. Take, and M. Bolton, "Measuring soil deformation in geotechnical models using digital images and PIV analysis," in *10th international conference on computer methods and advances in geomechanics*, Tucson, AZ, no. 1, pp. 997–1002, 2001.

[7] B. Wieneke, "Stereo-PIV using self-calibration on particle images," *Experiments in fluids,* vol. 39, no. 2, pp. 267–280, 2005.

[8] E. Y. Stepanov, V. Maslov, and D. Zakharov, "A stereo PIV system for measuring the velocity vector in complex gas flows," *Measurement*

Techniques, vol. 52, no. 6, p. 626, 2009.

[9] R. K. Shah and A. L. London, *Laminar flow forced convection in ducts: a source book for compact heat exchanger analytical data*. New York: Academic press, p. 3, 2014.

[10] S. Zou, T. Murayama, S. Motoda, S. Hara, and K. Inaoka, "Heat transfer of three-dimensional backward-facing step flow: local heat transfer coefficients on the bottom wall and upper wall," *The Harris science review of Doshisha University,* vol. 61, no. 2, pp. 125–131, 2020.

[11] K. Inaoka, K. Nakamura, and M. Senda, "Heat transfer control of a backward-facing step flow in a duct by means of miniature electromagnetic actuators," *International Journal of Heat and Fluid Flow,* vol. 25, no. 5, pp. 711–720, 2004, doi: 10.1016/j.ijheatfluidflow.2004.05.006